Amyloid precursor protein causes fusion of promyelocytic leukemia nuclear bodies in human hippocampal areas with high plaque load

David Marks
Ruhr University Bochum: Ruhr-Universitat Bochum
Natalie Heinen
Ruhr-Universität Bochum: Ruhr-Universitat Bochum
Lisa Bachmann
Ruhr-Universität Bochum: Ruhr-Universitat Bochum
Sophia Meermeyer
Ruhr University Bochum: Ruhr-Universitat Bochum
Michelle Werner
Ruhr-Universität Bochum: Ruhr-Universitat Bochum
Lucia Gallego Villarejo
Ruhr University Bochum: Ruhr-Universitat Bochum
Peter Hemmerich
Leibniz Institute on Aging: Leibniz Institut fur Altersforschung Fritz-Lipmann Institut eV
Verian Bader
Ruhr University Bochum: Ruhr-Universitat Bochum
Konstanze Winklhofer
Ruhr-Universität Bochum: Ruhr-Universitat Bochum
Elisabeth Schröder
Universität Duisburg-Essen: Universitat Duisburg-Essen
Shirley K Knauer
Universität Duisburg-Essen: Universitat Duisburg-Essen
Thorsten Müller (✉ thorsten.t.mueller@rub.de)
Ruhr-Universitat Bochum

Research article

Keywords: Alzheimer's disease, APP-CT; PML; iPSC-derived cerebral organoids, 3D culture; nuclear complexes; human brain; amyloidogenic plaques, HSV, viral defence

Posted Date: September 21st, 2020

DOI: https://doi.org/10.21203/rs.3.rs-74943/v1

Abstract

Background

The amyloid precursor protein (APP) is a type I transmembrane protein with unknown physiological function. Amyloidogenic processing of APP causes the generation of different cleavage products amongst b-amyloid and the APP C-terminal (APP-CT) fragment.

METHODS

1D, cerebral organoid 3D cell culture and human hippocampal post-mortem tissue were used to study APP-CT signalling in combination with immunofluorescence, -precipitation, confocal and STED imaging.

RESULTS

The current study demonstrates that APP-CT signals to the nucleus causing the generation of dynamic aggregates consisting of FE65 and the tumour suppressors p53 and PML. PML aggregates fuse over time depending on the APP nuclear signalling and complexes of the APP-CT/p53/PML and FE65 are present in the aged human post-mortem brain but not in cerebral organoids. Precise quantification revealed that AD brains show a significant loss of these nuclear aggregates in areas with high plaque load. The PML aggregates are co-localized to the herpes simplex virus in the human brain.

CONCLUSIONS

Our data show that APP-CT signalling recruits the nuclear PML body machinery and is of central relevance for neurodegeneration in AD with a potential function in viral defence.

Full Text

This preprint is available for download as a PDF.

Figures

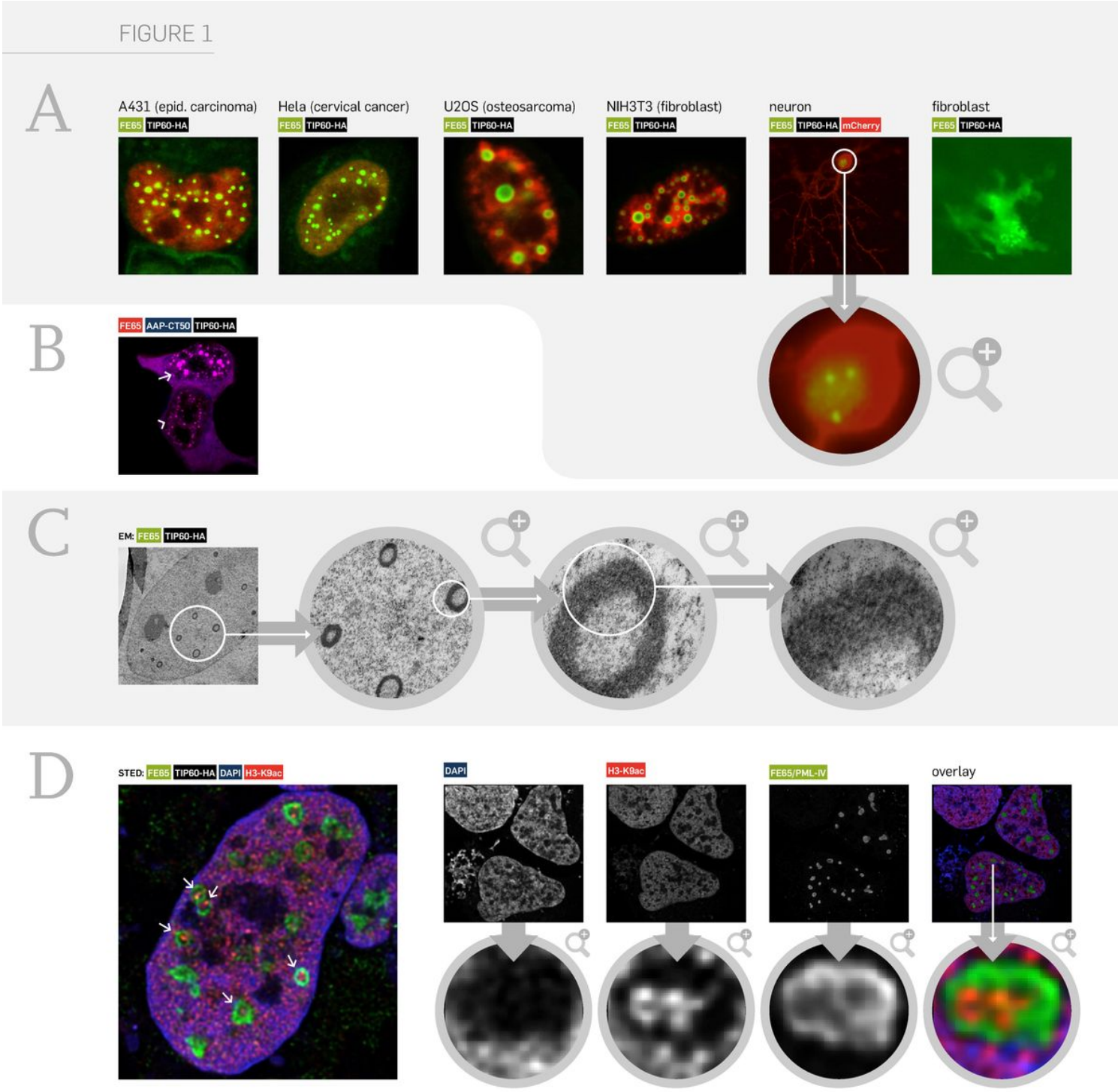

Figure 1

Dynamic nuclear APP-CT dependent aggregates are present in various cells, lack a membrane coating and are transcriptionally active. (A) Upon co-expression of FE65-mCherry/TIP60-EGFP, nuclear aggregates are generated in various cell lines including neurons. Transfected vectors with respective fluorophore (EGFP, mCherry) are indicated, TIP60 was co-transfected w/o fluorophore. (B) Every cell type used in A demonstrated cells with many tiny (arrow) or few large spheres (arrowhead) (or transition states) supporting the hypothesis of sphere fusion over time (blue, DAPI counterstain of nuclei; an overview image is also given in Supplement Figure S1). (C) Transmission electron microscopy of FE65/TIP60

transfected cells revealed an electron-dense ring structure (additional image in Figure S2). However, there was no evidence for a membrane sheath. These results were also confirmed by a CellMask staining (Supplement Figure S3). (D) High-resolution STED imaging revealed that the inner core of the aggregates is positive for anti K9 acetylation histone 3 antibody staining (red) supporting the hypothesis of active gene expression within the aggregates.

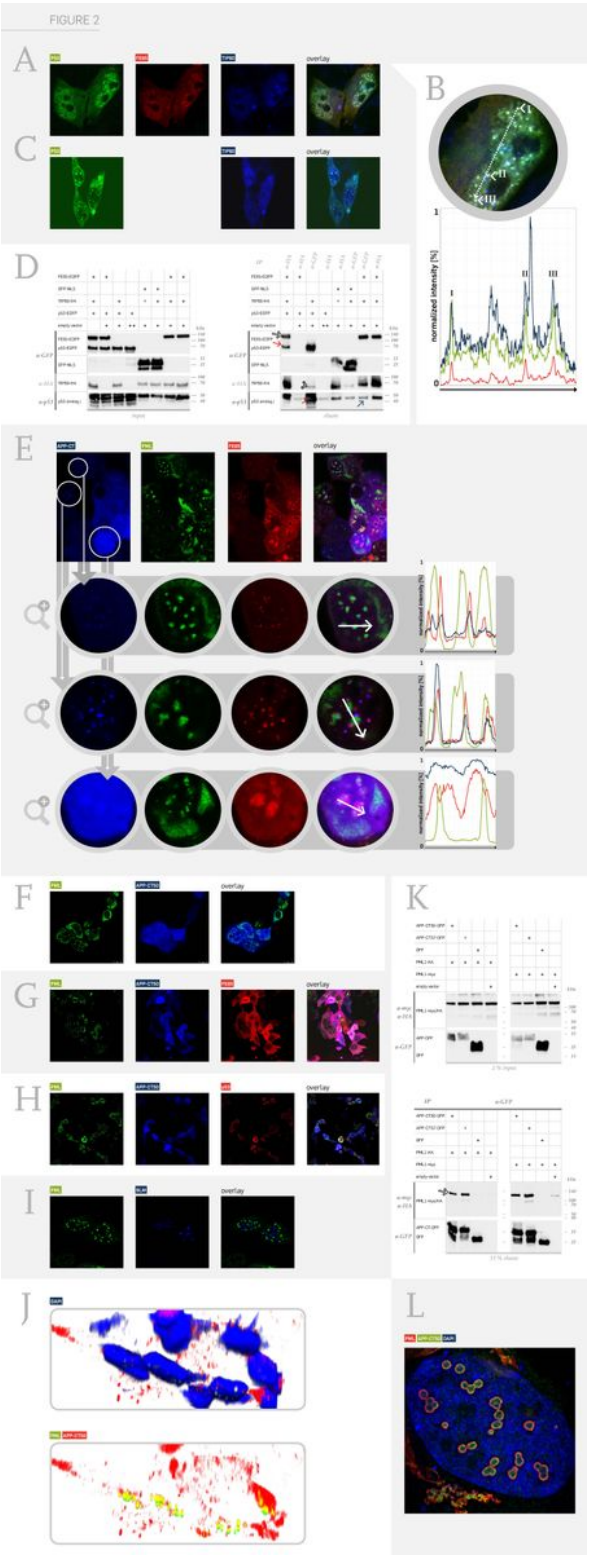

Figure 2

The nuclear APP-CT complex associates to p53 and PML. (A) The tumour suppressor protein p53 revealed the same nuclear dot-like structure as the co-transfected components FE65 and TIP60. Fluorescently labelled proteins are indicated in the Figure by the respective colour. (B) Tracking of the fluorescence intensity along the indicated arrow revealed peak intensities of each component (green: p53, red: FE65, blue: TIP60) supporting the association within one complex. (C) P53 is also co-localized to TIP60 independent of FE65. (D) P53 interaction with the APP-CT complex (FE65-EGFP/ TIP60-HA co-transfected to p53-EGFP vs. control (GFP-NLS, nuclear localization sequence)) was validated by co-immunoprecipitation (above: input blot, below: elution blot). IP using anti-HA tag antibody (against TIP60-HA) revealed precipitation of FE65 (white arrow) as well as of p53 (red arrow). Respective controls did not show a co-precipitation. TIP60 precipitation also occurred using anti-GFP as bait in well agreement to results obtained in part C (white arrowhead). Notably, high levels of endogenous p53 co-eluted in the same condition (red arrowhead), whereas a moderate endogenous p53 signal was observable in control conditions (red arrow). (E) A second tumour suppressor protein was identified to associate with the APP-CT complex: the promyelocytic leukemia protein PML. Different phenotypes of association were observed, e.g. one or two APP-CT/FE65 dots (TIP60 was co-transfected w/o fluorophore) associated with a single PML aggregate (first and second zoom-in row, compare fluorescence intensities). Alternatively, large APP-CT/FE65 complexes with enclosed PML-dots were found (third row). (F) A direct co-localization of APP-CT with PML was only observed to some extent (cells with nuclear aggregates), but most cells revealed a uniform staining pattern of APP-CT50 and PML in the cytosol and nucleus. (G) Additional co-expression of FE65 enriched the aggregation of PML in the nucleus, but a strong co-localization to APP-CT/FE65 was not observable in the imaging study. (H) p53 is part of the PML aggregates in the nucleus that also contain APP-CT. (I) Notably, the DNA helicase BLM, which was identified as binding protein in the APP-CT complex, is not co-localized with the PML aggregates. (J) Confocal 3D imaging validated the co-localization of PML and APP-CT in the nucleus (FE65/TIP60 were co-transfected). (K) Interaction of APP-CT with PML was shown using co-immunoprecipitation assay. Precipitation using anti-GFP antibody revealed detection of APP-CT-GFP (as expected) as well as PML (PML1 isoform was used, white arrow). This was true for two different APP-CT isoforms (APP-CT50 and CT57), whereas control conditions revealed no unspecific co-precipitation. Results were the same for two different PML1 tags: in the left panel of blots PML1-HA was used, whereas PML1-myc was used in the right panel. (L) High-resolution STED imaging specified the localization of APP-CT within the PML bodies. Different phenotypes were evident, either with a uniform localization within the bodies or with APP-CT signal at the inside wall of the PML body (red: PML, green: APP-CT).

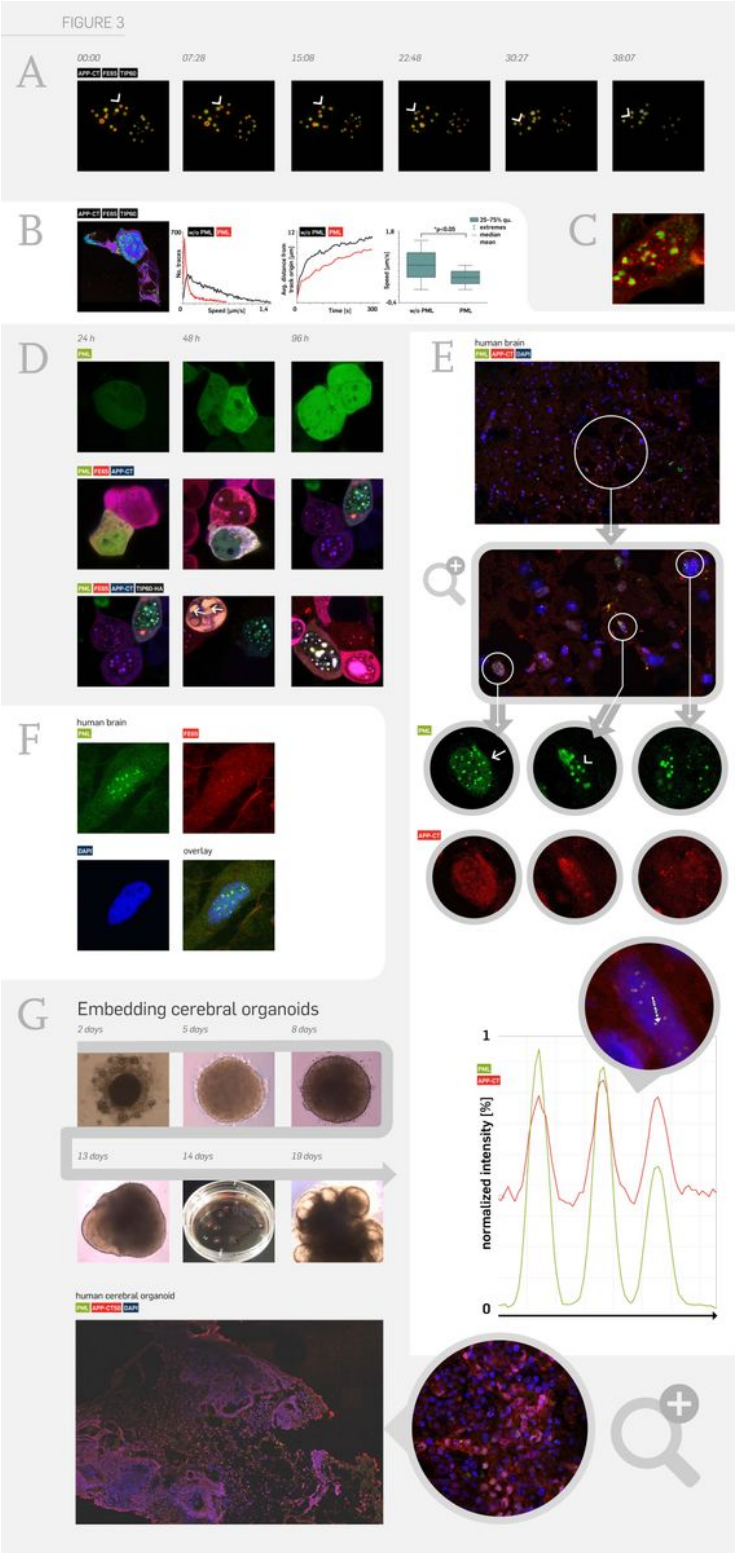

Figure 3

Highly mobile APP-CT-depending complexes that are also present in the aged human brain drive PML complex generation. (A) Expression of APP-CT/ FE65/TIP60 in HEK293 cells reveals a highly mobile complex moving three-dimensionally in the cellular nucleus. Ring-like structures were coloured (orange to yellow) according to z-level (confocal The indicated structure (white arrowhead) revealed time-dependent movement. (B) Movement of the individual aggregates was tracked using Huygens object tracker

software. Transfection in HEK293 cells included APP-CT/FE65-mCherry/TIP60 with and without GFP-PML co-expression. The FE65-mCherry signal was used for tracking, revealing lower speed in cells co-expressing PML (first diagram). In addition, the distance from the track origin (at time point 0) was analysed. Co-expression of PML revealed significantly lower distances pointing to mutual trapping of both complexes. The mean speed was 0.38 in PML vs. 0.76 µm/s in non-PML co-expressing cells (last diagram). (C) This part reveals a representative image demonstrating the complex generation of APP-CT/FE65/TIP60 (red) and PML (green aggregates). (D) Time-dependent generation of nuclear APP-CT/PML aggregates. EGFP-PML expression revealed a uniform distribution within the nucleus and cytosol (first row). Co-expression of FE65-mCherry and APP-CT caused initial aggregate formation after 48 h (middle row). Additional expression of TIP60 (last row) showed early generation of nuclear aggregates after 24 h. 48 h after transfection large nuclear aggregates were observed (white arrow). (E) PML/APP-CT co-localization was studied in human brain sections. In total, 15 human hippocampal sections were analysed (different Braak stages). Confocal tile-scan imaging (5 z-stacks, then fused by maximum projection algorithm) revealed strong co-localization of PML (green) with APP-CT (red). As in cell culture experiments, nuclei containing many small aggregates (arrow) as well as nuclei with larger aggregates (arrowhead) were evident. Co-localization is further shown by intensity tracking of both fluorescent channels in the diagram for a nucleus along the dotted white arrow. (F) Similarly, co-staining of PML and FE65, which confirmed the association of both proteins in the nuclei of the human brain, was performed. (G) In order to address the question whether co-localization also occurs in non-aged tissue, we differentiated human cerebral organoids from induced pluripotent stem cells. Embryonic bodies were embedded in Matrigel at day 11 followed by neuronal induction to generate organoids, which were analysed after 30 days in culture (seeding at day 0). Staining of cryosections failed to demonstrate co-localization of APP-CT and PML.

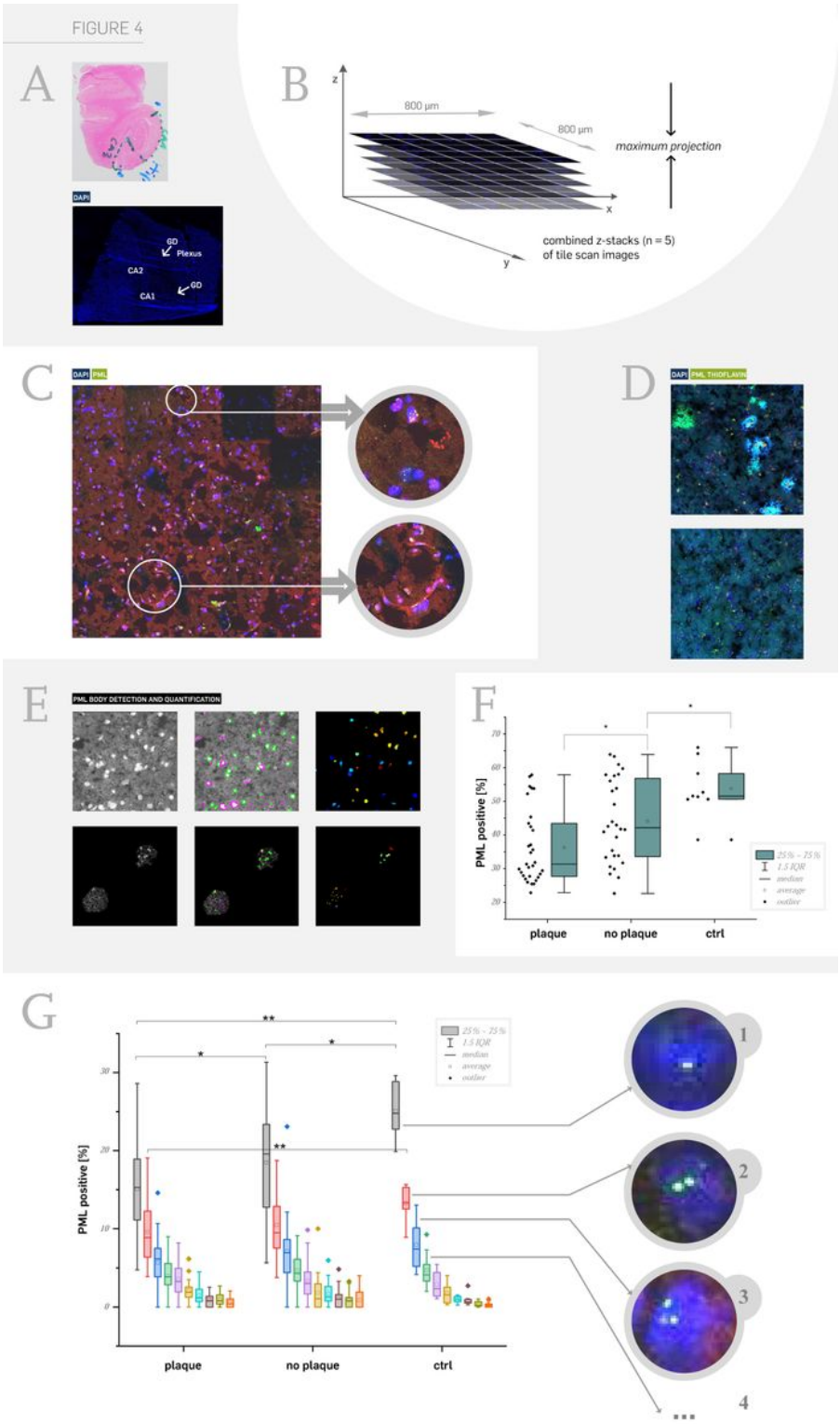

Figure 4

enrichment of PML bodies in human brain areas with high plaque load. (A) Haemotoxylin eosin (HE) staining of human hippocampal sections was used to define Cornu Ammonis (CA) 1-3, Gyrus dentatus (GD), and Plexus areal. Parallel sections were used for PML immunofluorescence staining. DAPI co-staining was used for low-resolution tile-scan imaging and allocation of specific CA areas according to the initial HE staining. (B) Hippocampal CA1 or CA3 areas were used for high-resolution tile scan imaging.

A single scan included 5x5 images with 5 z-stacks, which were subsequently combined using maximum projection. (C) A representative high-resolution (100x objective) confocal tile-scan image demonstrates identification of PML bodies in DAPI counter-stained nuclei. (D) Tile-scan imaging was then established with Thioflavin co-staining in order to identify areas with high plaque load in the human hippocampus (CA1 or CA3). (E) CellProfiler™ software was used to automatically annotate and extract nuclei (DAPI channel in grey scale) from the image (upper row). Subsequently, PML body identification and quantification was done in the extracted nuclei. (F) All nuclei containing 1 to 5 PML bodies were used to determine the percentage of PML positive nuclei (y axis). Hippocampal areas with high plaque load (plaque, average = 36.2 %) revealed a significant lower percentage of PML positive nuclei compared to areas without plaque (no plaque, average = 44.1 %) ($p<0.05$; every dot (left to each bar) indicates a single tile-scan experiment; for areas with high plaque load 31 tile-scans were analysed and quantified, 28 for no plaque, 9 for control). Tile-scans of control sections (individuals without any plaque pathology, average = 53.8 %) revealed again higher percentage of PML positive nuclei compared to “no plaque” areas ($p<0.05$). (G) Detailed analysis of cells containing one up to ten PML bodies per nucleus revealed significant differences. Nuclei with a single PML body were underrepresented ($p<0.05$) in areas with high plaque load vs. areas without plaques. Difference to control tile scans were highly significant ($p<10-5$). In addition, nuclei with two PML bodies (red bars) also revealed highly significant differences to the control. Representative images for nuclei containing one, two, or three PML bodies are given.

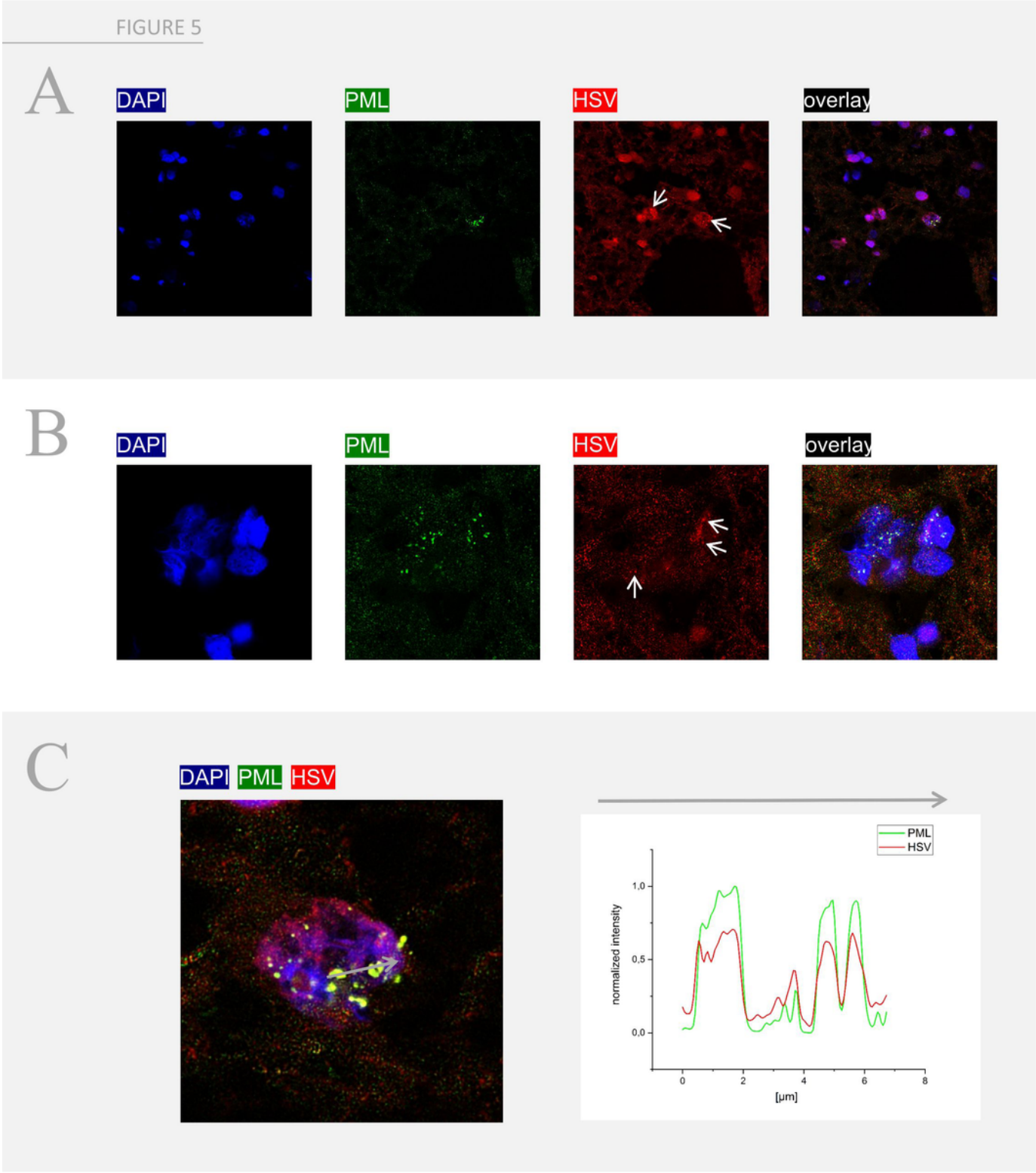

Figure 5

PML co-localizes to the herpes simplex virus. Human post-mortem brain sections were co-stained for HSV (red) using a labelled DNA probe and anti PML antibody (green). (A) Nuclear dots revealed co-localization for both signals, which was true for many cells within the human brain (B). Fluorescence intensity correlation of a cell demonstrating prominent PML dots (depicted from A) revealed the same course of fluorescence along the nuclear aggregates (grey arrow).

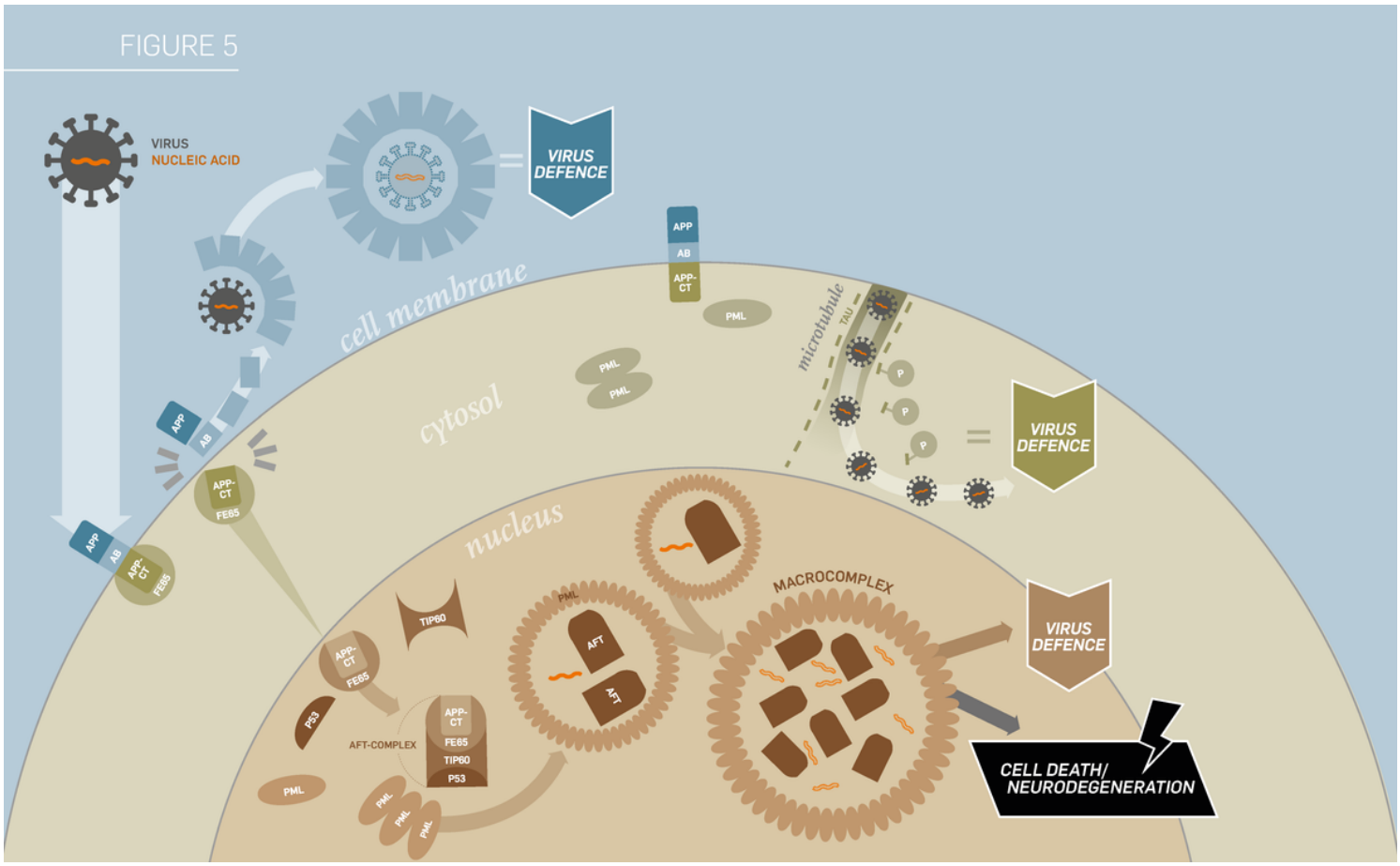

Figure 6

Hypothetical role of APP in virus defence. Our model suggests a twofold APP-related response to viral infection supported by our results and current literature as mentioned in the discussion. APP cleavage causes generation of β-amyloid, which has been shown to have antiviral relevance. The second defence mechanism is the sequestration of APP-CT, its signalling to the nucleus, and the generation of PML containing complexes. These AFT (APP-CT/FE65/TIP60)/PML aggregates might encapsulate viral nucleic acid preventing it from replication or initiating its degradation. However, overwhelming the response machinery due to repetitive infection (over years during live) or reduced immune system fitness might oblige the cell to degenerate as a last pyrrhic victory like defence strategy. Notably, the hyper-phosphorylation of TAU reducing the microtubule driven intracellular virus transport machinery might be associated to another virus defence strategy.